RSC Advances

ROYAL SOCIETY OF CHEMISTRY

www.rsc.org/advances

Journal Name

RSCPublishing

ARTICLE

Insights into the pore tuning of Triazine-based nitrogen-rich organoalkoxysilane membranes for use in water desalination

Cite this: DOI: 10.1039/xoxxoooooox

Received ooth January 2012,
Accepted ooth January 2012

DOI: 10.1039/xoxxoooooox

www.rsc.org/

Suhaina M. Ibrahim,[a,b] Rong Xu,[c] Hiroki Nagasawa,[a] Akinobu Naka,[e] Joji Ohshita,[d] Tomohisa Yoshioka,[a] Masakoto Kanezashi,[a] and Toshinori Tsuru[a]*

A promising new triazine-based nitrogen-rich organosilica (TTESPT) membrane has been developed for molecular separation processes in gas (gas separation) and liquid phases (reverse osmosis (RO)). By adjusting the H_2O/TTESPT molar ratio, we found a promising technique for tuning the pore network of TTESPT membranes. An increase in the H_2O/TTESPT molar ratio of from 60 to 240 fully hydrolyzed all the ethoxides groups in the TTESPT membrane, which reduced the size of the pores in the silica pore network. A TTESPT membrane with a high H_2O/TTESPT molar ratio exhibited a high degree of selectivity for H_2/SF_6 (greater than 4,000) at a permeation temperature of 200 °C. This membrane also demonstrated high sodium chloride (NaCl) rejection (>98.5%) with water permeability of >1 x 10^{-12} $m^3/(m^2\ s\ Pa)$ under operating conditions of 1 MPa and 60 °C during a RO experiment. As the operating temperature was increased from 25 to 60 °C, the NaCl rejection was constant without displaying the characteristic flux deterioration. This showed that the membrane retained a stable hybrid network structure.

Introduction

The desalination of seawater and brackish water has been practiced regularly for more than 50 years and is a well-established source of water supply in many countries. It is now feasible, technically and economically, to produce large quantities of water of an excellent quality from these desalination processes.[1] The major desalination technologies currently in use are based on membrane separation via RO and thermal distillation, with RO accounting for more than 50% of the installed capacity.[2-4] Because of its relatively lower energy cost and simplicity, RO is expected to see robust growth in the near future, though new technologies such as membrane distillation (MD),[5,6] electrodialysis,[5,7] capacitive deionization,[5,8] and forward osmosis[5,9] have been proposed.

At present, water desalination is accomplished using many types of membrane materials such as polymers and ceramics. Polymeric membranes such as polyamide and cellulose-based membranes for RO and polytetrafluoroethylene membranes for MD are commonly used due to their low cost, and ease of fabrication. However, the polyamide thin-film composite membranes are the most leading materials in the desalination industry due to their superior water flux, and a high degree of salt and organic rejection.[10-12] However, these membranes have some drawbacks. They often suffer from the swelling effect, have a short life-time due to bio fouling, have a narrow operating temperature (0 to 45 °C) and pH range, and are prone to chlorine attack.[12-14] Emerging materials made up of inorganic membranes such as zeolite and amorphous silica, on the other hand, are more resistant to harsh conditions.[10] Zeolites silica-based membranes have been studied extensively and because of their very specific pore structure and narrow pore size distribution, they have shown potential advantages for desalination.

Li et al.[15] reported on high chemical-stability silicalite membrane-based desalination. For a 0.1 M NaCl solution, a silicalite membrane of 1 nm pore diameter showed transient (time dependent) water flux and Na^+ rejections at 2.07 MPa. After a RO time of 50 h, the water flux and Na^+ rejections were stabilized at 0.112 kg/m^2 h and 76.7%. For a multiple-salt solution of 0.1 M NaCl, KCl, NH_4Cl, $CaCl_2$, and $MgCl_2$, the water flux was 0.058 kg/m^2 h, and the rejections of Na^+, K^+, NH_4^+, Ca^{2+}, and Mg^{2+} reached 58.1, 62.6, 79.9, 80.7, and 88.4%, respectively, at a RO pressure of 2.4 MPa. These results show that the filtration mechanism is not only dependent on size exclusion, but also on Donnan exclusion due to the charged double layer induced by ions adsorbed onto the pores or on the inter crystalline walls. Although the first RO test with a zeolite membrane was unsuccessful, i.e., both salt rejection and water flux were too low to be of practical use, subsequent work has been conducted to improve both by modifying the zeolite structure. The same research group also reported that defects in the crystal structure can be improved by incorporating aluminum ions into the zeolite framework; hence, both water flux and ion rejection was increased from 0.112 to 1.129 kg/m^2 h and ion rejection was improved from 90.6 to 92.9%.[16] Another recent study on MFI membranes showed that desalination performance of the prepared silicalite membrane was carried out with a seawater solution (0.3 wt% TDS (total dissolved solids)) for as long as 180 days at a

constant pressure of 700 kPa and at various temperatures. The prepared silicalite membrane achieved a high rate of rejection (>93%) for all major seawater ions, including Na^+ (except for K^+, 83%) at an applied pressure of 700 kPa and at room temperature (22 °C), but showed a continuous decrease in ion rejection when the temperature was increased from 22 to 90 °C. However, the permeation flux was significantly increased with an increase in temperature.[17]

Another promising candidate for use in RO desalination is an amorphous silica-based membrane. These materials are gaining in demand because of their simple fabrication techniques, low-cost and excellent molecular sieving properties. These membranes have shown superior performances in gas separation.[18-20] However, these membranes have a weakness due to structural instability when exposed to water, and probably undergo dissolution or densification.[21,22] Thus, the overall separation performance is decreased as a consequence, and the quality of the desalinated water drops. Therefore, alternative effort has been devoted to improving the hydrothermal stability of these silica membranes. Recently, a significant hydrothermal improvement was achieved when the siloxane bridges (Si-O-Si) were partially replaced by organic bridges (Si-CH_2-CH_2-Si) such as bis(triethoxysilyl)ethane (BTESE). These promising organosilica membranes had been studied in liquid and vapor separation (pervaporation)[23-25] and gas separation,[26,27] and were then extended to desalination (reverse osmosis).[28] Numerous generations of organoalkoxysilanes have emerged and been prepared as membranes via sol-gel processes such as bis(triethoxysilyl)methane (BTESM), 1,3-bis(triethoxysilyl)propane (BTESP), and the aromatic bridging groups: benzene and biphenyl.[29,30] Thus far, however, only BTESE and bis(triethoxysilyl)ethylene (BTESEthy) have been used in the preparation of RO membranes. According to Tsuru et al.[31] BTESE-derived organosilica membranes have shown superior retention performance for mono and bivalent ions and neutral solutes of low-molecular-weight, such as isopropyl alcohol and glucose. Compared with BTESE membranes, BTESEthy membranes,[32] with polarizable and rigid ethenylene bridges in the network structure have led to improved water permeability and high NaCl rejection (>98.5%). Both membranes have shown a tolerance of high temperatures.[31,32]

Therefore, the purpose of the present study was to introduce a new organoalkoxysilane- 2,4,6-tris[3-(triethoxysilyl)-1-propoxy]-1,3,5-triazine (TTESPT)-with triple silicon alkoxides and a triazine unit structure to determine its performance in an RO application. This material was chosen because we believed that the TTESPT membrane is more polarizable and attractive to water molecules compared with the BTESE and BTESEthy membranes. Recently, high CO_2 uptakes (≈ 38–51 cm^3/g) were obtained at ambient pressure and temperature using a new class of 1,3,5-triazine-based microporous polymers. The CO_2 uptake was enhanced by 70-90% when the polymers were carbonized at 400 °C for 1 h and at 800 °C for an additional 1 h under nitrogen.[33] Rabbani and El-Kaderi[34] also demonstrated that microporous polybenzimidazole containing nitrogen atoms had high CO_2 uptake capacity and selectivity over N_2 based on the interaction between N_2 atoms and CO_2 molecules. Thus, we expected TTESPT membranes to have similar adsorption properties towards selected gases and water molecules. In addition, we adjusted the H_2O/TTESPT molar ratio during the preparation of the TTESPT sols to tune the pore size of TTESPT membranes to achieve optimal desalination performance. To the best of our knowledge, we are the first to test the performance of TTESPT membranes in gas separation[35] and RO.

Experimental

Synthesis of 2,4,6-tris[3-(triethoxysilyl)-1-propoxy]-1,3,5-triazine (TTESPT)

In a 30 mL two-necked flask equipped with a stirrer and a reflux condenser, we placed 4.40 g (17.7 mmol) of 2,4,6-triallyloxy-1,3,5-triazine and 10.40 g (63.3 mmol) of triethoxysilane in 10 mL of toluene under an atmosphere of dry nitrogen. Two drops of 0.1 M H_2PtCl_6 in *i*PrOH were added, and the mixture was heated to reflux for 4 h. Excess triethoxysilane and toluene were removed under vacuum to give TTESPT as a colorless liquid (12.08 g): MS *m/z* 741 (M^+); ^{1}H NMR (δ $CDCl_3$) 0.69 (m, 6H, CH_2Si), 1.18 (t, 27H, CH_3, J = 7.0 Hz), 1.82-1.92 (m, 6H, CH_2), 3.78 (q, 18H, CH_2O, J = 7.0 Hz), 4.28-4.36 (m, 6H, CH_2O); ^{13}C NMR (δ $CDCl_3$) 6.40 (CH_2Si), 18.20 (CH_3), 22.18 (CH_2), 58.34 (OCH_2), 70.26 (OCH_2), 173.02 (triazine carbon).[35] The NMR spectra revealed some unidentified signals at low intensities, which were likely due to a partial hydrolysis of the TTESPT during the reaction and the workup process. Fig. 1 shows a schematic diagram of the synthesis of 2,4,6-tris[3-(triethoxysilyl)-1-propoxy]-1,3,5-triazine (TTESPT).

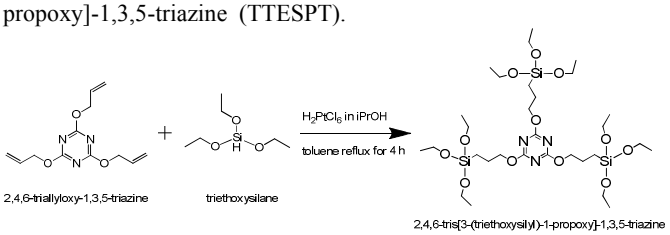

Fig. 1 Schematic diagram of the synthesis of 2,4,6-tris[3-(triethoxysilyl)-1-propoxy]-1,3,5-triazine (TTESPT).

Preparation of TTESPT organosilica sols and membranes

TTESPT as a silica precursor was homogeneously dissolved in an ethanol solution. A mixture of water and hydrochloric acid were then added dropwise to the solution under vigorous stirring, resulting in a final solution with molar ratios of TTESPT/H_2O/acid = 1/60/0.2 and 1/240/0.2. Then, the solution was kept in a closed system under continuous stirring at 25 °C for 6 h to allow the formation of silica sols. Porous α-alumina tubes (porosity: 50%, average pore size: 1 μm, outside diameter: 10 mm) were used as the supports for TTESPT-derived silica membranes. α-Alumina particles (average particle diameter: 0.2, 1.9 μm) were coated onto the outer surface of a porous support using a silica-zirconia colloidal sol as the binder, and the support was fired at 550 °C for 30 min to smooth the surface. These procedures were repeated several times to cover large pores that might have resulted in pinholes in the final membrane. Then, a SiO_2–ZrO_2 (Si/Zr = 1/1) solution (diluted to about 0.5 wt%) was coated onto the substrate to form an intermediate layer with pore sizes of several nm, followed by calcination at 550 °C for approximately 30 min. Finally, the TTESPT-derived silica layer was fabricated by coating a TTESPT solution, followed by drying and calcination at 300 °C under nitrogen for 30 min.

Characterization of TTESPT organosilica sols and membranes

The sizes of freshly prepared TTESPT sols in a 10% dilution in ethanol were measured by dynamic light scattering (DLS) Zetasizer Nano (Malvern, ZEN3600) at 25 °C. Thermogravimetric analysis (TG) was performed to investigate the decomposition behavior of the organic groups in the silica matrix at temperatures ranging from 100 to 1,000 °C with a heating rate of 10 °C min^{-1} in a helium flow of 300 ml min^{-1} using a thermogravimetric analyzer (TGA-DTA-

PIMS 410/S, Rigaku, Japan). A N_2 adsorption isotherm was obtained at 77 K to study the micropore structures of the silica gels. Prior to the measurement, all the silica gel samples were evacuated at 150 °C for 12 h. The measurements were carried out using BELMAX software (BEL JAPAN INC., Japan). The morphologies of the TTESPT membranes were examined using a Hitachi S-48000 field emission scanning electron microscope (FESEM).

Performance Evaluation of the TTESPT membranes

Single-Gas Permeation

Fig. 2 shows a schematic diagram of the experimental apparatus for the single-gas permeation measurement. Gas permeation tests were performed at 200 °C using single components of He, H_2, CO_2, N_2, CH_4, C_3H_6, C_3H_8, and SF_6. The permeation stream was maintained at atmospheric pressure, and the pressure drop through the membranes was maintained at 1 bar. Prior to the measurement, all membranes were outgassed in a He flow of 50 ml min^{-1} at 200 °C for 8 to 12 h to remove any water that had possibly adsorbed on the membranes.

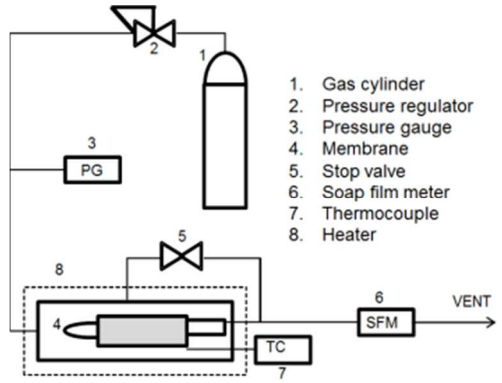

Fig. 2 Schematic diagram of the experimental apparatus for single gas permeation measurement.

Reverse Osmosis Performance Test

The RO experiment was conducted in a cross-flow filtration system, as shown in Fig. 3. The feed solution was pressurized with a plunger pump at a pressure of 1 MPa, and a temperature of 25 °C was maintained unless otherwise specified. The retentate was recycled back to the feed container while the permeate stream was maintained at atmospheric pressure and collected using a microtube pump. The concentrations of feed solutions were 2,000 ppm of NaCl, and 500 ppm of ethanol, isopropanol, and glucose. The concentrations of feed and permeate were measured with a conductivity meter (HORIBA, ES-51) for electrolytes and a total organic carbon analyzer (Shimadzu, TOC-VE) for neutral solutes. Performance evaluation of the RO membrane was conducted via the calculation of water permeability, L_p, and observed rejection, R. Water permeability, L_p, was calculated from the volume flux J_v divided by the effective transmembrane pressure, $\Delta P - \Delta\pi$.

$$L_p = J_v/(\Delta P - \Delta\pi) \quad (1)$$

For sufficiently dilute solutions, the osmotic pressure difference, $\Delta\pi$, for NaCl was determined using the van't Hoff equation:[36]

$$\Delta\pi \cong 2RT(C_f - C_p) \quad (2)$$

where R is the gas constant, T is the absolute temperature, C_p is the permeate concentration, and C_f is the feed concentration. The effect of concentration polarization was rationally ignored in this work due to low permeate flux. An observed rejection, R, was expressed as follows:

$$R\ (\%) = (1-C_p/C_f) \times 100 \quad (3)$$

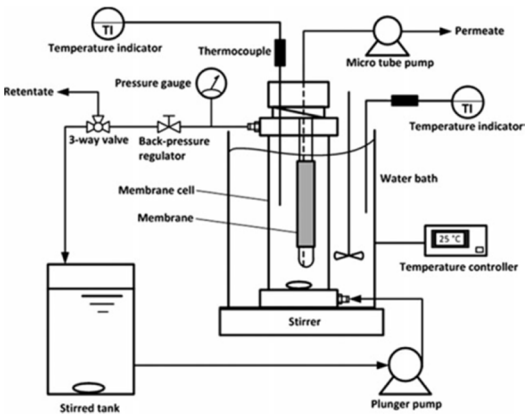

Fig. 3 Schematic diagram of the experimental apparatus for reverse osmosis measurement.

Results and discussion

Characterization of TTESPT sols, powders and membranes

To study the effect of the H_2O/TTESPT molar ratio, two different molar ratios, 60 and 240, were prepared. Theoretically, increasing the amount of water content can encourage bond formation and create an open fractal polymer, which is needed to attain molecular sieving ability.[23,37] Fig. 4 shows the size distributions of the TTESPT sols determined by dynamic light scattering at 25 °C. The TTESPT-60 and TTESPT-240 were used to denote TTESPT sols prepared at H_2O/TTESPT molar ratios of 60 and 240, respectively. In this work, the TTESPT-60 sol produced a small sol size of 0.8 nm. On the contrary, the TTESPT-240 sol exhibited a sol size of approximately 2.3 nm, which was slightly larger than the former sol. This phenomenon can be related to a faster rate of the hydrolysis reaction. The increment of the sol size distribution was probably dominated by the polymerization reaction of monomer species, instead of the aggregation reaction. If an aggregation of nanoparticles occurred, it would result in a dramatic increment of sol size distribution compared with the sizes that are shown in Fig. 4.[38-40]

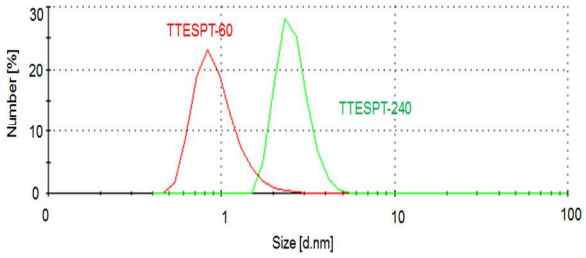

Fig. 4 Colloidal size distribution of the TTESPT sols at 25° C.

Fig. 5 shows the TG curves of TTESPT-60 and TTESPT-240 powders as a function of temperature. As shown in Fig. 5, analysis of the TG curves for both samples indicated that thermal decomposition occurred in two steps. The same observation was reported by other researchers for a new class of 1,3,5-triazine-based microporous polymer sample that was conducted under an N_2 atmosphere.[33] Two degradation steps occurred during the TG analysis: the first degradation stage occurred in temperatures that ranged from 100 to 310 °C, while the second stage was observed in temperatures that ranged from 310 to 650 °C. The first degradation stage can be ascribed to the evaporation of adsorbed water, solvent, acid and the decomposition of unreacted ethoxy groups, and also to the partial decomposition of some branching bonds of triazine units in the powder.[41] The second degradation stage for TTESPT-60 and TTESPT-240 occurred at temperatures that ranged from ~310 to 650 °C; this may correspond to the pyrolysis of cleavage of the C-C, C-O, C-N and C=N branching bonds of the TTESPT units induced by thermal treatment. The decomposition of these bonds signifies that CH_4, CO_2, CH_3CN, and H_2 were generated.[33,41,42]

The N_2 adsorption isotherms and pore size distribution of TTESPT powders after calcination at 300 °C, are shown in Fig. 6. In accordance, Table 1 summarizes the specific surface area for both powders. It is possible that different amounts of water content exhibited significant changes within the isotherm patterns and pore size distributions. TTESPT-60 powder displayed a non-porous isotherm forming pores with an average size that ranged from 1.9 to 20 nm, or larger. This may have been due to the unreacted ethoxide groups that blocked the pore mouth of the silica network. Moreover, triazine units may have acted as "building blocks" between the silica pores, and occupied some space in the silica network, resulting in a limited number of open pores and a lower surface area. On the contrary, the adsorption branch of TTESPT-240 powder seems to have been a combination of Type I and IV isotherms. Therefore, as the water content increased, some micropores were created by the hydrolysis and condensation reaction. The pore diameters for TTESPT-240 powder ranged from 0.6 to 1.7 nm, and, hence, the surface area was increased, showing that the TTESPT-240 was more porous than the TTESPT-60. A schematic diagram of TTESPT pore networks with a different H_2O/TTESPT molar ratio appears in Fig. 7. Obviously, increasing the H_2O/TTESPT molar ratio can stimulate the formation of a network of smaller pores in a TTESPT membrane due to a higher degree of cross-linking. Fig. 8 shows the cross-section of a SEM image of a TTESPT membrane. This clearly shows that a crack-free, continuous separation layer was formed on the top of the SiO_2-ZrO_2 and alumina layers after the calcination process at 300 °C.

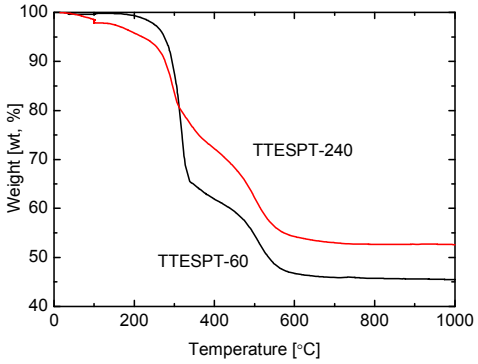

Fig. 5 TG curves of TTESPT-derived silica gel powder (Ramping rate: 10 °C min^{-1}; He flow rate: 300 ml min^{-1}).

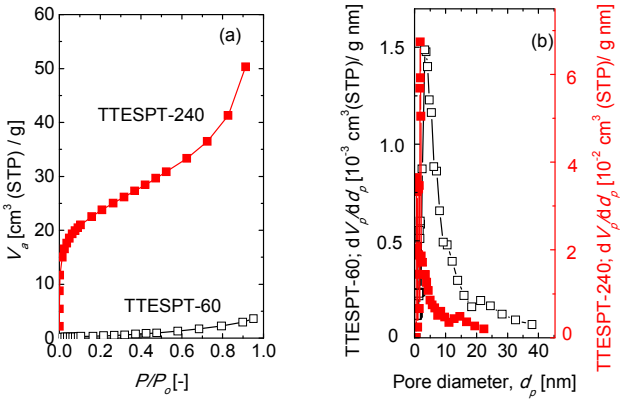

Fig. 6 (a) N_2 Adsorption and (b) Pore size distribution of TTESPT-silica gel powders.TTESPT-60 (open keys) and TTESPT-240 (closed keys).

Table 1 Summary of the surface area for TTESPT membranes calcined at 300 °C.

Membranes	Surface Area [m^2/g]
TTESPT-60	2
TTESPT-240	80

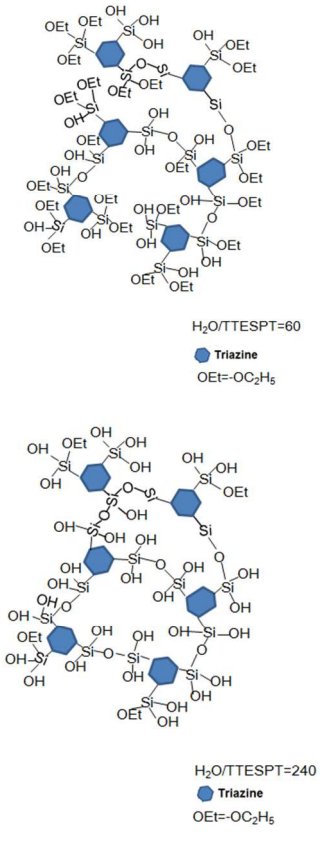

Fig. 7 Schematic diagram of the effect of the H_2O/TTESPT molar ratio on a TTESPT pore network.

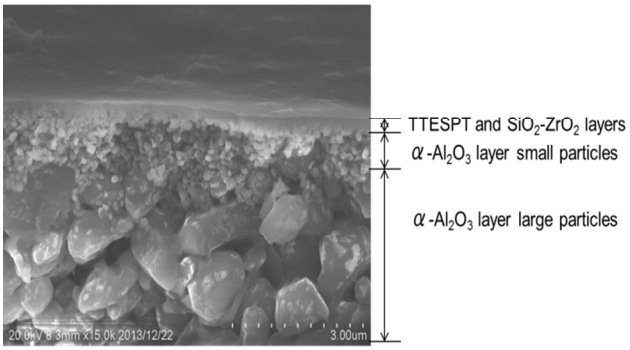

Fig. 8 Cross-sectional SEM image of a TTESPT membrane calcined at 300 °C.

Gas Permeation Properties of TTESPT membranes

To investigate the separation efficiency of a TTESPT membrane calcined at 300 °C, gas permeation was conducted at a permeation temperature of 200 °C using He, H_2, CO_2, N_2, C_3H_6, C_3H_8, and SF_6, as shown in Fig. 9 (a). It is noteworthy that both TTESPT membranes exhibited a H_2 permeance of higher than 10^{-6} mol/(m^2 s Pa), but a moderate H_2/N_2 selectivity of approximately 9 to 14, as shown in Table 2. On the other hand, the H_2/SF_6 selectivity for the TTESPT-60 membrane was approximately 720 and was increased drastically (to 4,700) by increasing the H_2O/TTESPT molar ratio to 240. Arrhenius plots of the gas permeances observed for TTESPT-60 and TTESPT-240 membranes are supplied in the Electronic Supporting Information-1 (ESI-1) manuscript. The gas permeances for both membranes increased with the permeation temperature, revealing that the activated diffusion transport mechanism was dominant.

In order to quantitatively evaluate the pore size of these membranes, a normalized Knudsen-based permeance (NKP) method was applied.[41] This NKP method was based on a modified gas translation (GT) model that was derived by modifying the original GT model proposed by Xiao and Wei[43] and by Shelekhin et al.[44] for the determination of membrane pore sizes of less than 1 nm. A more detailed explanation of this model can be found elsewhere.[41] NKP is the ratio of the permeance of the *i-th* component to that predicted with He, which is the smallest molecule, under the Knudsen diffusion mechanism. The expression for normalized Knudsen-based permeance can be obtained as follows.

$$NKP = \frac{P_i\sqrt{M_i}}{P_{He}\sqrt{M_{He}}} = \frac{(d_p - d_{k,i})^3}{(d_p - d_{k,He})^3} exp\left(-\frac{E_{p,i} - E_{p,He}}{RT}\right) \quad (4)$$

where $d_{k,i}$ is the molecular size of the *i*-th component and d_p is the average pore size of the membrane. The activation energy of the *i-th* and He components, the gas constant, and the temperature are denoted as $E_{p,i}$, $E_{p,He}$, R and T, respectively. In the present study, for simplicity, the assumption of a negligible difference in the activation energy of permeation was made, in order to easily evaluate the pore sizes of microporous membranes, leading to the following expression for NKP (eq 5).

$$NKP = \frac{(d_p - d_{k,i})^3}{(d_p - d_{k,He})^3} \quad (5)$$

Fig. 9 (b) shows the NKP plot at 200 °C where the effect of surface flow can be negligible. It seems the pore size of TTESPT-derived silica membranes obtained via the NKP method shifted from a large to a small size, i.e., from 8 to 5 Å, when the H_2O/TTESPT molar ratio was increased from 60 to 240. This was because the TTESPT-240 membrane structure consisted of a smaller pore network compared with the TTESPT-60 membrane. One possible reason was due to the high degree of cross-linking that occurred in the TTESPT-240 membrane. As the H_2O/TTESPT molar ratio increased, the 9 ethoxy groups in TTESPT-240 should have been fully hydrolyzed and formed silanol groups. These silanol groups were then condensed with one another to form siloxane bonds that created a network of progressively smaller pores, as shown in Fig. 7.

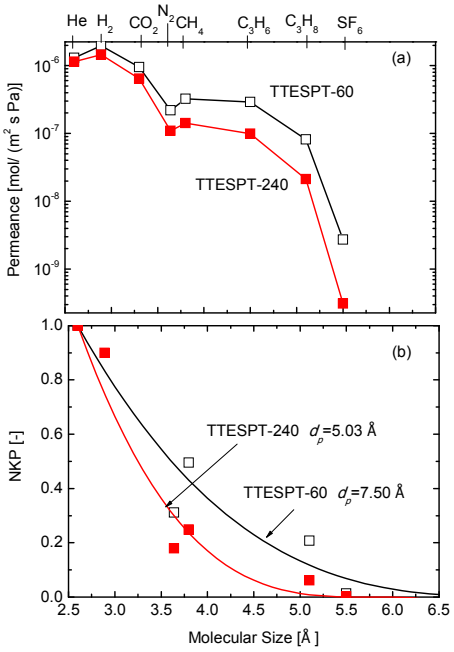

Fig. 9 (a) Gas permeation properties **(b)** Normalized Knudsen-based permeance (NKP) of TTESPT-derived silica membranes calcined at 300 °C at a permeation temperature of 200 °C as a function of molecular size: TTESPT-60 (open keys) and TTESPT-240 (closed keys).

Table 2 Summary of Gas Permeance and Selectivity at 200 °C for TTESPT membranes.

Membranes	Permeance [10^{-9} mol/(m^2 s Pa)]			Selectivity	
	H_2	N_2	SF_6	H_2/N_2	H_2/SF_6
TTESPT-60	1970	218	2.72	9.0	722
TTESPT-240	1460	109	0.30	13.3	4725

In our previous manuscript,[35] we reported that TTESPT-derived silica membranes calcined at different calcination temperatures (200, 300 and 400 °C) exhibited an outstanding degree of selectivity for adsorptive molecules such as C_3H_6 and C_3H_8 at permeation temperatures of 50 °C, as shown in Table 3. In general, the C_3H_6/C_3H_8 selectivity decreases with increasing C_3H_6 and C_3H_8 permeance as a result of defects or variations in the pore size distribution. Interestingly, the separation performances of TTESPT-derived silica membranes calcined at 200 °C showed similar properties to carbonized membranes. Meanwhile, the separation performance of TTESPT-derived silica membranes calcined at temperatures of 300 and 400 °C showed similar or better separation properties than BTESM and Titanosilicate membranes at permeation temperatures that ranged from 50-200 °C. This tendency could be attributed to the presence of the π-bond (C=C double bond) in propene, which can have an affinity for the hydroxyl groups of silica

and –C=N- triazine units. The superior sieving ability and adsorption affinity of TTESPT membranes motivated us to study its desalination performance.

Table 3 Summary of C_3H_6 permeance and selectivity for C_3H_6/C_3H_8 at a permeation temperature of 50 °C for TTESPT-derived silica membranes H_2O/TTESPT=240.

Calcination temperatures [°C]	C_3H_6 Permeance [10^{-9} mol/(m^2 s Pa)]	C_3H_6/C_3H_8 Selectivity [-]
200	2.95	37
300	59.8	8
400	305	7

Reverse osmosis properties of TTESPT membranes

Fig. 10 shows the molecular weight cut-off (MWCO) curves of the TTESPT membranes determined by RO experimentation using neutral solutes with different molecular weights (MW) at 1 MPa and 25 °C. As shown in Fig. 10, rejection increased in an ascending order of the molecular weight of solutes. Both membranes showed a quite high degree of rejection for neutral solutes of low molecular weight. Rejections for all the neutral solutes are as follows: ethanol, 38% (TTESPT-60) and 43% (TTESPT-240); isopropanol, 80% (TTESPT-60) and 90% (TTESPT-240); and, glucose, >98% (both TTESPT-60 and TTESPT-240). The values for MWCO, determined at a 90% rejection for TTESPT-60 and TTESPT-240 membranes, were estimated to be approximately 110 and 60, respectively. Stokes diameters for ethanol, isopropanol and glucose were 0.4, 0.48 and 0.73 nm, respectively.[45] Therefore, it was suggested that the rejection of the solutes had occurred mainly based on the molecular sieving effect. Table 4 compares the pore sizes of TTESPT membranes estimated by the different methods. Apparently, small pore sizes exhibited smaller MWCO values, indirectly, suggesting that the separation performance was strongly induced by molecular sieving.

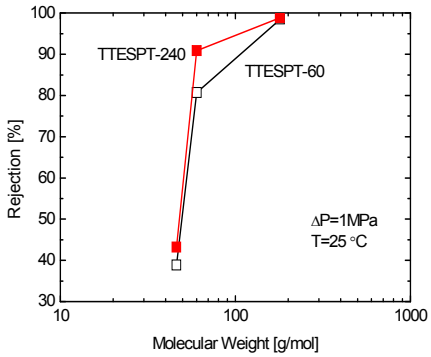

Fig. 10 MWCO curves of TTESPT membranes.

Table 4 Comparison of the pore sizes of TTESPT membranes.

	TTESPT-60	TTESPT-240
N_2 Adsorption (nm)	>1.9 to 20	0.6 to 1.7
NKP calculation (Å)	8	5
MWCO (g/mol)	110	60

Water permeability and NaCl rejection capability was used to assess the desalination performance of TTESPT membranes. The RO desalination performance was evaluated using a 2,000 ppm NaCl solution at pressures that ranged from 0.4 to 1 MPa at 25 °C. Fig. 11 shows the effect of feed pressure on the permeation of water and salt rejection using TTESPT membranes. The water flux (J_v) of both membranes increased simultaneously as operating pressure increased, whereas the water permeability (L_p) was almost constant, confirming that the pressure difference was the only driving force of water permeation. As the pressure increased, the enhanced water permeation led to an increase in salt rejection in TTESPT-60 and TTESPT-240 membranes that ranged from 93 to 96% and 95 to 98%, respectively. This can be easily explained by a solution-diffusion (SD) model that can be found elsewhere.[31] According to this model, the water permeation was influenced by the operating pressure, but the ion permeation was not. The TTESPT-240 membrane exhibited a higher rejection but a lower water flux than the TTESPT-60 membrane due to the small-sized pore networks that were formed in this membrane.

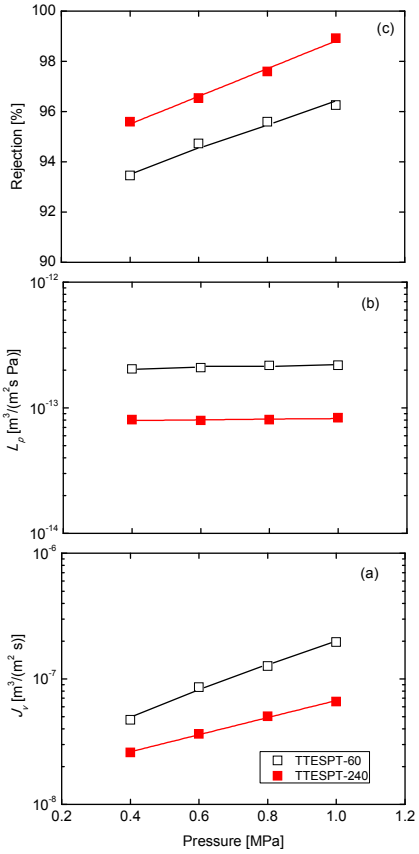

Fig. 11 (a) Water flux, J_v, (b) Water permeability, L_p, and (c) Rejection, R, as a function of pressure at 25 °C and 2,000 ppm NaCl: TTESPT-60 (open keys) and TTESPT-240 (closed keys).

Fig. 12 illustrates the schematic image of water transport through the amorphous silica networks of a TTESPT membrane. It is acknowledged that the transport mechanism of water and NaCl during RO is influenced by a molecular sieving phenomenon, which is the same as that of single-gas permeation. Hence, a TTESPT membrane must possess a pore size that falls between that of ions and water in order to increase its suitability for molecular sieving (ion rejection). The hydrated sizes of $Na^+_{(aq)}$, $Cl^-_{(aq)}$ and H_2O are 0.72, 0.66 and 0.276 nm, respectively.[17] On the other hand, the

molecular sizes of helium, hydrogen and SF_6 gases are 0.26, 0.289 and 0.55 nm, respectively. Therefore, it is reasonable to use helium or hydrogen gases as a predictor of water permeance and SF_6 gas as a predictor for NaCl permeance. The H_2/SF_6 selectivity for the TTESPT-60 membrane was approximately 720 and was increased drastically (to 4,700) by increasing the H_2O/TTESPT molar ratio to 240, resulting in smaller MWCO and higher NaCl rejection. The TTESPT-240 membrane was believed to consist of dense silica networks and small pores compared to the TTESPT-60 membrane. Thus, it should be possible to estimate the rejection of NaCl molecules by comparing the selectivities of either He/SF_6 or H_2/SF_6.

As mentioned earlier, the application of a variation in the H_2O/TTESPT molar ratio, succeeded in tuning the pore size of TTESPT membranes. A rough estimation of the pore sizes of these TTESPT membranes via NKP demonstrated that high water content produced a smaller pore size. This enhancement of water permeability for the TTESPT-60 can be fully explained by this phenomenon. Larger pore size may accommodate more water molecules being transported continuously through the membrane, but the rejection status will be lowered. On the other hand, a smaller pore size will exert a strong blocking effect that will reject NaCl ions, thus inhibiting water molecules from entering the membrane pores and lowering the water flux.

The water permeation performance of the membranes as a function of temperature is shown in Fig. 13 (a-d). The water permeability increased approximately 10-fold as the operating temperature increased from 25 to 60 °C, as shown in Fig. 13 (a). The Hagen-Poiseuille equation (6) below was employed to theoretically estimate the permeability through porous membranes.

$$L_p\mu = r_p^2 A_k / 8\Delta x \quad (6)$$

where r_p is the effective pore size, Δx is the effective membrane thickness, and A_k is the porosity.

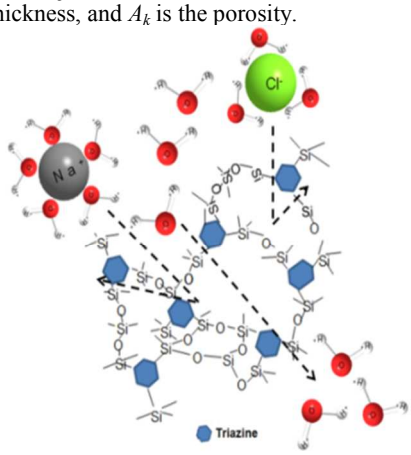

Fig. 12 Schematic images of water transport through the amorphous silica networks of a TTESPT membrane.

If the transport mechanism obeys the viscous flow mechanism, the viscosity-corrected water permeability, $L_p\mu$, should remain constant with the origin, despite the permeation temperature. As shown in Fig. 13 (b), the values for the $L_p\mu$ of both TTESPT membranes were not constant and clearly increased with temperature. Therefore, the transport mechanism through TTESPT membranes was confirmed to deviate from the viscous flow mechanism. The transport mechanism through the TTESPT membranes may be attributed to an activated transport mechanism, which is typical for microporous materials. Hence, for further investigation into the effect of temperature on permeability, the $L_p\mu$, was normalized at 25 °C for the TTESPT membranes and at 30 °C for the TiO_2 membrane,[46] as shown in Fig. 13 (c). Obviously, the normalized $L_p\mu$ for the membranes was increased as temperature increased. However, the steepness of the line increases in corresponding to the order of TTESPT-240>TTESPT-60>TiO_2. From Fig. 13 (a) and (b), the observed activation energies of $\Delta E(L_p)$ and $\Delta E(L_p\mu)$ can be obtained using the Arrhenius equations below.

$$L_p = (L_p)_o \exp(-\Delta E(L_p)/RT) \quad (7)$$
$$L_p\mu = (L_p\mu)_o \exp(-\Delta E(L_p\mu)/RT) \quad (8)$$

where ΔE, R and T, are the the activation energy of the membrane, the gas constant, and the temperature, respectively.

Table 5 summarizes the values of the observed activation energies of L_p and $L_p\mu$ for each membranes. The observed activation energies of each membrane increased with decreasing pore size and MWCO values, which is in agreement with an activated transport mechanism. Since the average pore size of the TTESPT membranes was smaller than that of the TiO_2 membranes, water molecules were expected to exert strong friction against the pore walls. As the temperature increased, the water molecules with sufficient energy could break through the energy barrier to be transported through the TTESPT micropore networks. Another possible reason could have been the adsorption of water on the membrane pore wall. It is believed water adsorption to the hydrophilic portions of the TTESPT pore wall were governed by the bonds of Si-OH, C=N, and C-N groups. On the other hand, the rejection of TTESPT membranes seemed to have been constant or even increased (Fig. 13 (d)), which confirmed that the pore sizes of these membranes were not influenced by the thermal expansion in the present operating temperature range. Although similar temperature dependence for water permeability was reported for polymeric membranes,[47,48] this had been attributed to the enlargement of the pore size due to thermal expansion during the high-temperature conditions, which lowered the rate of rejection.

In order to investigate the membrane hydrothermal durability, both TTESPT membranes were evaluated for 30 hours at temperatures that ranged from 25 to 60 °C at 1 MPa with 2,000 ppm NaCl. As shown in Fig. 14 (a) and (b), the water permeabilities for TTESPT-60 and TTESPT-240 membranes were more than 1 x 10^{-12} $m^3/(m^2\ s\ Pa)$ and showed excellent salt rejection of >96 and 98%, respectively, at operating conditions of 1 MPa and 60 °C. The water permeabilities increased as the operating temperature increased. It was noteworthy that the rejection remained unchanged over time and temperature. This result fully supported the idea mentioned above that the increment of water permeability was due to activated diffusion whereas passage through the membrane of the NaCl ions was still hindered due to the small sizes of the pores in the TTESPT membrane network. These results also suggest that no alteration of the effective pore diameters and structures occurred. The excellent thermal stability can be attributed to the main body of the TTESPT structure that consisted of chemically strong bonds such as Si-C and Si-O-Si. To substantiate this fact, FTIR analysis was done to investigate the TTESPT structure after the RO thermal experiment. Fig. 15 shows that most of the peaks of the TTESPT membrane remained nearly the same with no significant changes or structural deterioration before and after the RO thermal experiment. Therefore, it was confirmed that the TTESPT membrane had an inherently stable organosilica network and structure. Table 6 summarizes the comparisons of the desalination performances of different types of

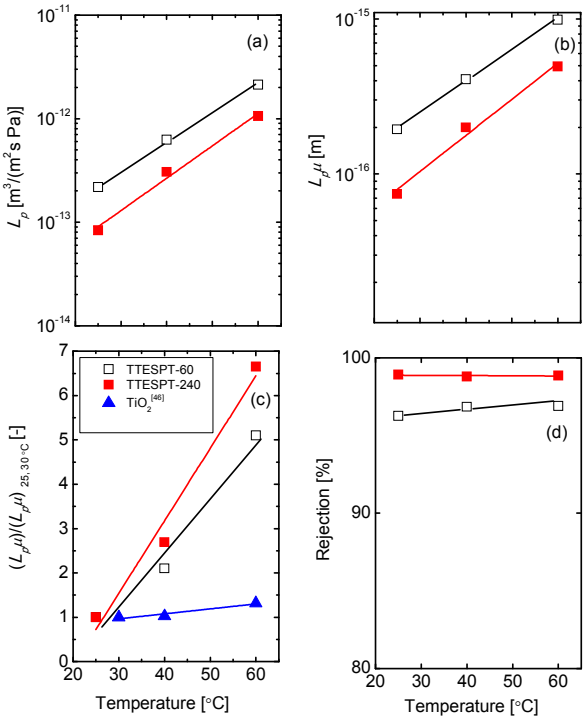

Fig. 13 (a) Water permeability, L_p, (b) Viscosity-corrected water permeability, $L_p\mu$, (c) Normalized viscosity-corrected water permeability, $L_p\mu$, and (d) Rejection, R, as a function of temperature at 1 MPa and 2,000 ppm NaCl: TTESPT-60 (open keys), TTESPT-240 (closed keys) and TiO_2 (triangle closed keys).

Table 5 Activation Energies of L_p and $L_p\mu$ for TTESPT and TiO_2 membranes.

Membranes	TTESPT-60	TTESPT-240	TiO_2-1000[46]
MWCO	110	60	1000
ΔE (L_p) (kJ/mol)	53.6	59.7	19.7
ΔE ($L_p\mu$) (kJ/mol)	38.4	44.5	5.1

membranes. Currently, interfacial polymerized polyamide membranes are the industry standard in this area as they exhibit superior water flux and salt rejection.[49] However, organosilica membranes shows only a moderate degree of water permeance with a high degree of rejection. Generally speaking, as we compared the performance of organosilica membranes with other zeolite membranes such as ZSM-5,[16] silicalite[50] and graphene[51] membranes, organosilica membranes can still be considered a high performance membrane, as shown in Table 6. If we narrow the comparison to the temperature dependency of organosilica membranes, the water permeability and salt rejection of TTESPT membranes displayed exactly the same characteristic as BTESE and BTESEthy membranes.[28,32] Obviously, TTESPT membranes can be considered one of the choices for water desalination. Table 7 summarizes the observed activation energies of L_p and $L_p\mu$ for all organosilica membranes. It is notable that smaller pore sizes exhibit larger activation energies. TTESPT membranes showed a larger degree of activation energies compared with the other two membranes even though the MWCO value was nearly the same. This was because the TTESPT membrane exhibited dual characteristics ascribable to organic (the flexibility via high chain mobility) and inorganic (Si-O-Si backbone that provides structural stability) groups. However, both BTESE and BTESEthy represent a rigid structure. Fig. 16 shows the schematic images of the BTESE and TTESPT membranes. According to Castrium et al.,[29] polymer material usually exhibits an increased diffusivity at higher temperatures, and this is related to an increased mobility of the organic chains. The TTESPT material consists of three long arms of propene groups that are connected to silicon alkoxides. The permeance through this material may have a similarity to the temperature-dependent chain mobility. This is in agreement with the findings in our previous manuscript[35] revealing that an activated diffusion transport mechanism was dominant for this material.

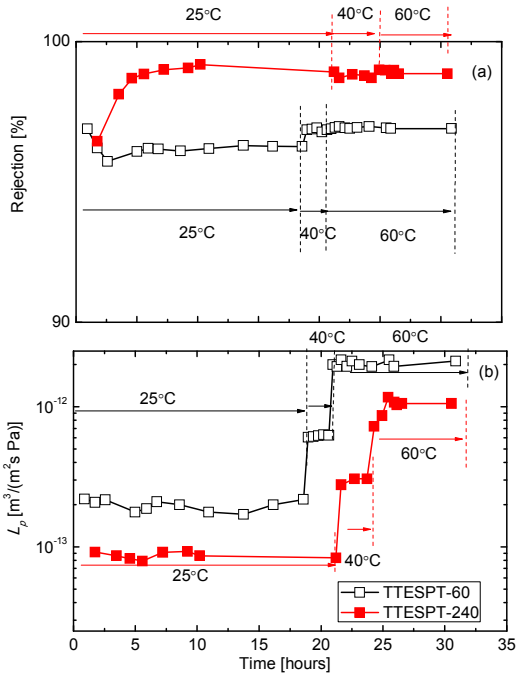

Fig. 14 (a) Salt rejection, R, and (b) Water permeability, L_p, for TTESPT membranes as a function of temperature at 1 MPa and 2,000 ppm NaCl.

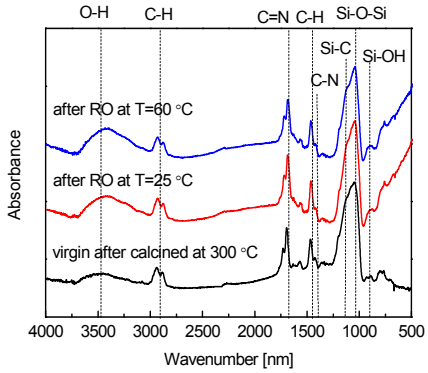

Fig. 15 FTIR spectra of the TTESPT membranes: virgin and after the RO thermal experiment at 25 and 60 °C.

Journal Name

RSCPublishing

ARTICLE

Table 6 Comparisons of the desalination performance of different types of membranes.

Membranes	Operating Condition	Water Permeability [$m^3/(m^2 s\ Pa)$]	Rejection [%]	Ref.
NaA-TFC Polyamide	1.6 MPa; 25 °C; 2000 ppm NaCl	5.6×10^{-12}	98	[49]
Silicate 1-TFC Polyamide	1.6 MPa; 25 °C; 2000 ppm NaCl	1.3×10^{-11}	96	[49]
ZSM-5, Si/Al=50	2.7 MPa; 25 °C; 0.1 M NaCl	1.4×10^{-13}	92	[16]
Silicalite	2.7 MPa; 25 °C; 0.1 M NaCl	4.3×10^{-14}	99	[50]
Ultrathin Graphene Nano-filtration	0.5 MPa; 0.02 M NaCl	None	40	[51]
BTESE	1.15 MPa; 25 °C; 2000 ppm NaCl	1.0×10^{-13}	97	[28]
	1.15 MPa; 60 °C; 2000 ppm NaCl	2.2×10^{-13}	98	[28]
BTESEthy	1.15 MPa; 25 °C; 2000 ppm NaCl	2.0×10^{-13}	98	[32]
	1.15 MPa; 60 °C; 2000 ppm NaCl	1.0×10^{-12}	98	[32]
TTESPT-60	1 MPa; 25 °C; 2000 ppm NaCl	2.2×10^{-13}	96	This
	1 MPa; 60 °C; 2000 ppm NaCl	2.2×10^{-12}	96	work
TTESPT-240	1 MPa; 25 °C; 2000 ppm NaCl	8.3×10^{-14}	98	This
	1 MPa; 60 °C; 2000 ppm NaCl	1.0×10^{-12}	98	work

Table 7 Summary of MWCO and Activation Energy of L_p and $L_p\mu$ for TTESPT, BTESE and BTESEthy membranes.

Membranes	TTESPT-240	BTESE[28]	BTESEthy[32]
MWCO	60	50	50
ΔE (L_p) (kJ/mol)	59.7	30.8	30.7
ΔE ($L_p\mu$) (kJ/mol)	44.5	15.3	15.7

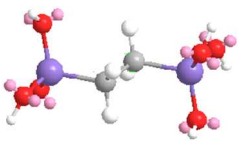

(a)

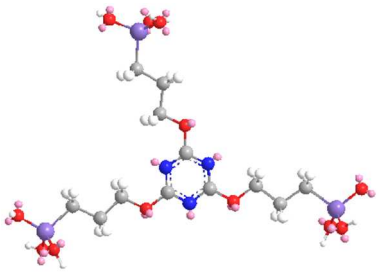

(b)

Fig. 16 Schematic images of (a) BTESE (b) TTESPT membranes.

In addition, the high water permeability, L_p, for a TTESPT membrane was likely due to high water affinity for the hydrophilic portions of the TTESPT pore wall that consisted of polar Si-OH, C-O, C=N and C-N groups. This was proven by quantum chemical calculations at the level of B3LYP/6-31G (d) using a Gaussian09 program. Fig. 17 shows the optimized geometry and electrostatic potentials of the TTESPT model simplified by replacing the ethoxy units on the silicon atoms with methoxy groups. The electrostatic potentials (ESPs) derived from the calculations also are depicted in Fig. 17, and these closely relate the electron density distribution. The colors ranged from -0.04 to +0.01 with red and blue denoting extremely electron rich and deficient regions, respectively. Clearly, the ESPs of this monomer model show that negative potentials are mainly localized on the C-O, C=N and C-N groups, while the non-polar C-H groups bear relatively positive potentials.

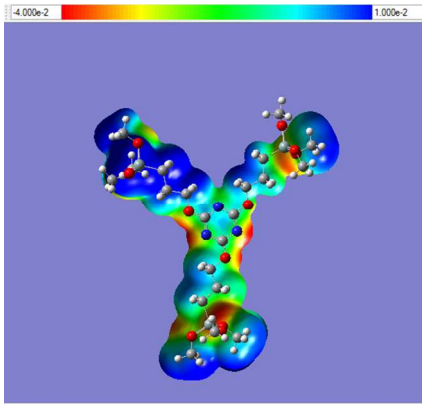

Fig. 17 Optimized geometry and electrostatic potentials of the TTESPT model, derived from DFT-calculations at B3LYP/6-31G(d).

Conclusions

In conclusion, the present study marks the first successful preparation of a TTESPT membrane that exhibits dual characteristics that are both organic (the flexibility via high chain mobility) and inorganic (Si-O-Si backbone that provides structural stability). By adjusting the H_2O/TTESPT molar ratio, the permeation properties of this membrane were enhanced. A higher H_2O/TTESPT molar ratio seemed to exhibit a smaller pore network membrane with high separation factors for H_2/SF_6 (>4,000) and salt rejection almost constant (>98%) with increases in the operating temperature that ranged from 25-60 °C at 1 MPa. It was evident that the variation of sol gel parameters such as the water ratio played an important role in the separation properties of the TTESPT membranes. Thus, further study on long-term stability under robust conditions (temperature, pH, etc.) and variations in salt rejection for the TTESPT membrane would be important.

Acknowledgements

This research is supported in part by Core Research for Evoluional Science and Technology (CREST) Program of Japan Science and Technology Agency (JST).

References

1 S. Otles and S. Otles, *Electron. J. Environ., Agric. and Food Chem.*, 2004, **4**, 963–969.
2 M. A. Shannon, P. W. Bohn, M. Elimelech, J. G. Georgiadis, B. J. Marin and A. M. Mayes, *Nature*, 2008, **452**, 301-310.
3 Y. Zhou and R. S. J. Tol, *Wat. Resour. Res*., 2005, **41**, 1–10.
4 S. Veerapaneni, B. Long, S. Freeman, and R. Bond, *J. Am. Water Works Assoc*., 2007, **99**, 95–106.
5 K. P. Lee, T. C. Arnot, and D. Mattia, *J. Membr. Sci.*, 2011, **370**, 1–22.
6 S. T. Hsu, K. T. Cheng, J. S. Chiou, *Desalin*., 2002, **143**, 279–287.
7 M. Sadrzadeh, and T. Mohammadi, *Desalin.*, 2008, **221**, 440–447.
8 Y. Oren, *Desalin.*,2008, **228**, 10–29.
9 R. L. McGinnis and M. Elimelech, *Desalin.*, 2007, **207**, 370–382.
10 M. Elma, C. Yacou, D. K. Wang, S. Smart and J. C. D. da Costa, *Water*, 2012, **4**, 629-649.
11 L. F. Greenlee, D. F. Lawler, B. D. Freeman, B. Marrot, and P. Moulin, *Water Res.*, 2009, **43**, 2317–2348.
12 D. Li and H. Wang, *J. Mater.Chem.*, 2010, **20**, 4551–4566.
13 H. B. Park, B. D. Freeman, Z. B. Zhang, M. Sankir and J. E. McGrath, *Angew. Chem. Int. Ed*., 2008, **120**, 6108–6113.
14 R. J. Petersen, *J. Membr. Sci*., 1993, **83**, 81–150.
15 L. Li, J. Dong,T. M. Nenoff, and R. Lee, *J. Membr. Sci.*, 2004, **243**, 401–404.
16 L. Li, N. Liu, B. McPherson, and R. Lee, *Ind. Eng. Chem. Res.*, 2007, **46**, 1584-1589.
17 B. Zhu, Z. Hong, N. Milne, C. M. Doherty, L. Zhou, Y. S. Lin, A. J. Hill, X. Gu, and M. Duke. *J. Membr. Sci.*, 2014, **453**, 126-135.
18 R. Igi, T. Yoshioka, Y. H. Ikuhara, Y. Iwamoto, and T. Tsuru, *J. Am. Ceram. Soc.*, 2008, **91**, 2975–2981.
19 T. Tsuru, R. Igi, M. Kanezashi, T. Yoshioka, S. Fujisaki, and Y. Iwamoto, *AIChE J.*, 2011, **57**, 618–629.
20 C. Yacou, S. Smart, and J. C. D. da Costa, *Energy Environ. Sci.*, 2012, **5**, 5820–5832.
21 R. Leboda, and E. Mendyk, *Mater. Chem. Phys.* 1991, **27**, 189–212.
22 M. C. Duke, J. C. D. da Costa, D. D. Do, P. G. Gray and G. Q. Lu, *Adv. Funct. Mater.*, 2006, **16**, 1215–1220.
23 H. L. Castricum, A. Sah, R. Kreiter, D. H. A. Blank, J. F. Vente and J. E. tenElshof, *J. Mater. Chem.*, 2008, **18**, 2150–2158.
24 H. L. Castricum, R. Kreiter ,H. M. vanVeen, D. H. A. Blank, J. F. Vente, and J. E. ten Elshof, *J. Membr. Sci.*, 2008, **324**, 111–118.
25 H. M. van Veen, M. D. A. Rietkerk, D. P. Shanahan, M. M. A. vanTuel, R. Kreiter, H. L. Castricum, J. E. tenElshof, and J. F. Vente, *J. Membr. Sci*., 2011, **380**, 124–131.
26 M. Kanezashi, K. Yada, T. Yoshioka, and T. Tsuru, *J. Am. Chem. Soc.*, 2009, **131**, 414–415.
27 M. Kanezashi, K. Yada, T. Yoshioka, and T. Tsuru, *J. Membr. Sci.*, 2010, **348**, 310–318.
28 R. Xu, J. Wang, M. Kanezashi, T. Yoshioka, and T. Tsuru, *Langmuir*, 2011, **27**, 13996–13999.
29 H. L. Castricum, G. G. Paradis , M. C. Mittelmeijer-Hazeleger, R. Kreiter , J. F. Vente , and J.E. ten Elshof, *Adv. Funct. Mater.* 2011, **21**, 2319-2329.
30 M. Kanezashi, M. Kawano, T. Yoshioka, and T. Tsuru, *Ind. Eng. Chem. Res*. 2012, **51**, 944-953.
31 R. Xu, J. Wang, M. Kanezashi, T. Yoshioka, and T. Tsuru, *AIChE J.*, 2013, **59**, 1298-1307.
32 R. Xu, M. Kanezashi, T. Yoshioka, T. Okuda, J. Ohshita, and T. Tsuru, *Appl. Mater. Interfaces.*, 2013, **5**, 6147-6154.
33 H. Lim, M. C. Cha, and J. Y. Chang, *Macromol. Chem. Phys.,* 2012, **213**, 1385−1390.
34 M. G. Rabbani and H. M. El-Kaderi, *Chem. Mater.*, 2011, **23**, 1650–1653.
35 S. M. Ibrahim, R. Xu, H. Nagasawa, A. Naka, J. Ohshita, T. Yoshioka, M. Kanezashi and T. Tsuru, *RSC Adv.*, 2014, **4**, 12404-12407
36 M. L. Lind, D. E. Suk, T. V. Nguyen, and E. M. V. Hoek, *Environ. Sci. Technol*. 2010, **44**, 8230-8235.
37 O. Lev, K. Tsionsky, L. Rabinovich , V. Glezer, S. Sampath, I. Pankratov, and J.Gun, *Anal. Chem*., 1995, **67**, 22A-31A.
38 R. S. A. Delange, J. H. A. Hekkink, K. Keizer and A. J. Burggraaf, *J. Non-Cryst. Solids*, 1995, **191**, 1-16.
39 D. R. Azolin, C. C. Moro, T. M. H. Costa, and E. V. Benvenutti, *J. Non-Cryst. Solids*, 2004, **337**, 201–206.
40 Y. Ma, M. Kanezashi, and T. Tsuru, *J. Sol-Gel Sci. Technol.*, 2010, **53**, 93–99.
41 H. R. Lee, M. Kanezashi, Y. Shimomura, T. Yoshioka, and T. Tsuru, *AIChE J.*, 2011, **57**, 2755-2765.
42 M. Kanezashi, M. Kawano, T. Yoshioka, and T. Tsuru, *Ind. Eng. Chem. Res.*, 2012, **51**, 944–953.
43 J. Xiao and J. Wei, *Chem. Eng. Sci.*,1992, **47**, 1123-1142.
44 A. B. Shelekhin, A. G. Dixon, and Y. H. Ma., *AIChE J*., 1995, **41**, 58-67.
45 X. L. Wang, T. Tsuru, S. Nakao, and S. Kimura, *J. Membr Sci.*, 1997, **135**, 19–32.
46 T. Tsuru, K. Ogawa, M. Kanezashi, and T. Yoshioka, *Langmuir*, 2010, **26**, 10897–10905.
47 N. B. Amar, H. Saidani, J. Palmeri, and A. Deratani, *Desalin.*, 2009, **246**, 294–303.
48 H. Saidani, N. B. Amar, J. Palmeri, and A. Deratani, *Langmuir*, 2010, **26**, 2574–2583.
49 H. Huang, X. Qu, X. Ji, X. Gao, L. Zhang, H. Chena and L. Hou, *J. Mater. Chem. A*, 2013, **1**,11343- 11349.
50 N. Liu, L. X. Li, B. McPherson, and R. Lee., *J. Membr Sci.,* 2008, **325**, 357–361.
51 Y. Han, Z. Xu, and C. Gao, *Adv. Funct. Mater.*, 2013, **23**, 3693-3700.

Notes and references

[a] Department of Chemical Engineering, Hiroshima University, 1-4-1 Kagamiyama, Higashihiroshima, 739-8527, Japan

[b] Advanced Material Research Centre (AMREC), SIRIM Berhad, Lot 34, Jalan Hi-Tech 2/3, Kulim Hi-Tech Park, 09000 Kulim, Kedah, Malaysia
[c] School of Petrochemical Engineering, Changzhou University, Changzhou, 213164, China
[d] Department of Applied Chemistry, Hiroshima University, 1-4-1 Kagamiyama, Higashihiroshima, 739-8527, Japan
[e] Department of Life Science, Kurashiki University of Science and the Arts, 2640 Nishinoura, Tsurajima, Kurashiki, Okayama 712-8505, Japan
, 2000, **35**, 3523.